Title- Undecaprenyl Pyrophosphate Phosphatase (UppP) is a pivotal element in *Salmonella* Intramacrophage Survival

Rhea Vij[1], Debapriya Mukherjee[1#], Kirti Parmar[1#], Dipshikha Chakravortty[1,2*]

[1]Department of Microbiology and Cell Biology, Indian Institute of Science, Bangalore 560012, India.

[2]Adjunct Faculty, Indian Institute of Science Research and Education, Thiruvananthapuram, Kerala, India

[#]Equal contribution

[*]Corresponding author: dipa@iisc.ac.in

Tel: 0091 80 2293 2842

Fax: 0091 80 2360 2697

Abstract

To establish infection, *Salmonella* confronts a dynamic barrage of host-induced stresses. The peptidoglycan layer, essential for maintaining cell integrity and counteracting environmental stress, relies on the lipid carrier undecaprenyl phosphate, generated by Undecaprenyl pyrophosphate phosphatase (UppP). While UppP is linked to virulence in other pathogens, its role in *Salmonella* remains unclear. We show that an *uppP* mutant in *S*. Typhimurium exhibits altered cell morphology, reduced stiffness, and impaired survival in RAW 264.7 macrophages. The mutant is also attenuated in systemic infection in C57BL/6 mice. These defects are associated with increased sensitivity to nitrosative stress. Notably, iNOS inhibition or deficiency restores intracellular survival of the *uppP* mutant in both RAW 264.7

macrophages and the mouse model, implicating UppP in resistance to nitrosative stress. Our findings reveal a moonlighting role for UppP in promoting *Salmonella* survival within macrophages and contributing to systemic pathogenesis.

Introduction

Salmonella is a Gram-negative foodborne pathogen belonging to the *Enterobacteriaceae* family [1]. The genus, comprising more than 2600 serovars, can infect various hosts, including plants, birds, and mammals[2], [3]. Clinical manifestations of *Salmonella* infection range from self-limiting gastroenteritis associated with non-typhoidal serovars to systemic infection caused by typhoidal serovars and invasive non-typhoidal serovars [4]. The significant burden of *Salmonella*-associated enterocolitis, affecting 95.1 million people in 2017, coupled with the rising threat of drug-resistant strains as recognised by its inclusion on the WHO priority pathogen list, underscores *Salmonella*'s growing danger to public health [5], [6], [7].

Salmonella enters the host through contaminated food and water. *Salmonella* encounters several stresses inside the host, such as oxidative, nitrosative stress, acidic pH, nutrient starvation, metal ions, and host antimicrobials [8]. The bacterial peptidoglycan layer helps counter these stresses by acting as a barrier to the external environment. It also helps in maintaining the bacterial shape and virulence. The synthesis of the peptidoglycan layer is a concerted effort of many proteins and takes place in the cytosolic and periplasmic compartments of the bacterial cell [9]. Biosynthesis of the peptidoglycan building block- N-acetyl glucosamine-N-acetyl muramyl-pentapeptide takes place in the cytoplasm, on the lipid carrier undecaprenyl phosphate (C_{55}-P), forming Lipid II, which is then flipped by MurJ or FtsW to the periplasmic phase[9], [10]. In the periplasmic phase, the disaccharide

pentapeptide part of Lipid-II undergoes polymerisation by Penicillin-binding proteins (PBPs) for peptidoglycan synthesis, releasing undecaprenyl pyrophosphate [11]. The undecaprenyl pyrophosphate (C_{55}-PP) is dephosphorylated by undecaprenyl pyrophosphate phosphatase (UppP) to undecaprenyl phosphate, which is utilised for another round of peptidoglycan synthesis [12]. Also, the newly synthesised undecaprenyl pyrophosphate in the cytoplasm by undecaprenyl pyrophosphate synthetase (UppS) from isopentyl diphosphate precursors serves as a substrate for UppP [12], [13].

Multiple studies have highlighted the crucial role of UppP in the virulence and pathogenesis of different bacterial species. In *E. coli*, *uppP*, known as *bacA*, overexpression leads to bacitracin resistance, as bacitracin strongly binds to undecaprenyl pyrophosphate and prevents its dephosphorylation [14]. Mutant strains lacking the *bacA* homologue in *Staphylococcus aureus* and *Streptococcus pneumoniae* exhibited reduced virulence and severe attenuation, respectively, in the mouse model of infection [15]. Other reports have shown that deletion of *uppP* in *Mycobacterium smegmatis* impairs its ability to form biofilms [16]. However, the role of undecaprenyl phosphate in *Salmonella* Typhimurium (STM) pathogenesis has remained unexplored.

In this study, we generated an *uppP* knockout strain of *S.* Typhimurium and evaluated its impact on bacterial survival and virulence. Intracellular *Salmonella* actively remodels its peptidoglycan layer to evade immune signalling, accentuating the plasticity of the bacterial cell wall during infection [17]. UppP's crucial function in peptidoglycan synthesis suggests that it may play a role in cell wall adaptation during stress, thereby enhancing *Salmonella*'s survival. Our findings demonstrate that UppP is essential for *S.* Typhimurium proliferation in RAW 264.7 macrophages and systemic dissemination in C57BL/6 mice by promoting resistance to host-induced nitrosative stress.

Results

UppP affects bacterial cell dimensions and strength

To investigate the role of undecaprenyl pyrophosphate phosphatase in *Salmonella* pathogenesis, we generated an *uppP*-deleted strain of *Salmonella* Typhimurium by a one-step chromosomal gene inactivation method [18]. We observed that the *uppP* deleted strain demonstrated no significant difference in growth in nutrient-rich LB broth (Fig. 1A), M9 minimal media (Fig. 1B) and acidic F-media (pH-5.4, similar to the pH of the SCV [19], [20]) (Fig. 1C).

A continuous supply of undecaprenyl phosphate is crucial for normal cell shape maintenance in *Escherichia coli*, and its production causes morphological defects [21], [22], [23]. To dissect the contribution of UppP in bacterial cell morphology of *Salmonella*, we performed Scanning Electron Microscopy (SEM) to examine the logarithmic and stationary-phase cultures of STM WT and STM Δ*uppP*. The quantitative analysis of cell length revealed that STM Δ*uppP* exhibits reduced cell length during the log phase but increased cell length during the stationary phase (Fig. 1D-E, S1A-B). Furthermore, we performed atomic force microscopy (AFM) to evaluate the bacterial cell strength. Young's modulus, quantified from AFM micrographs, was reduced in STM Δ*uppP* than in the wild type (Fig. 1F-G). Our results are indicative of *uppP*'s contribution to the maintenance of bacterial cell size and strength.

uppP plays a role in the intracellular survival of *Salmonella* in RAW 264.7 macrophages

As macrophages are key for *Salmonella* dissemination and produce a hostile environment for *Salmonella*, we performed an intracellular survival assay in RAW 264.7 cells and found that STM *ΔuppP* exhibits impaired invasion and fold proliferation (Fig. 2A, S2A). Since the intestinal epithelial barrier is *Salmonella*'s initial point of contact, we also evaluated the intracellular survival of STM *ΔuppP* in Caco-2 cells. However, we observed no significant

difference in the invasion or fold proliferation of STM *ΔuppP* compared to WT in Caco-2 cells (Fig. S2B-C).

As SPI-1 can also contribute to macrophage invasion [24], we evaluated the transcript levels of SPI-1 genes. We observed increased *sipA* (SPI-1 effector), *invF*, *hilA* (transcriptional regulators), and *prgH* (structural translocon component) transcripts in the mutant during both the logarithmic and stationary phase (Fig. S2D-E). Increased expression of SPI-1 genes is also associated with macrophage apoptosis during *Salmonella* infection [25], [26], [27]. We hypothesised that the reduced invasion and fold proliferation of STM *ΔuppP* may be attributed to the infected cells undergoing apoptosis. To evaluate the same, 16 hours post-infection, RAW 264.7 cells were treated with tetracycline, followed by an MTT assay to determine cell viability. No significant difference was observed in the cell viability between the wild-type, mutant and uninfected control (Fig. S2F). This suggests that apoptosis, or other forms of cell death, may not account for the decreased invasion and proliferation of STM Δ*uppP*.

Salmonella Pathogenicity Island (SPI)-2 is a key player in governing *Salmonella* survival in macrophages [28]. Since STM Δ*uppP* exhibited reduced fold proliferation in RAW 264.7 macrophages, we evaluated the transcript levels of SPI-2 effectors *sifA* and *spiC*. Interestingly, STM Δ*uppP* exhibited elevated transcripts of *sifA* and *spiC* during the stationary phase, compared to the wild-type (Fig. S2G).

Multiple host defences within the macrophage, such as acidic pH, reactive oxygen species, reactive nitrogen species, antimicrobial peptides, nutrient deprivation, etc, influence *Salmonella* survival [8]. We assessed the susceptibility of STM Δ*uppP* to exogenous stresses of hydrogen peroxide, nitrite and peroxynitrite by a resazurin dye-assisted cell viability assay. Despite exhibiting elevated reactive oxygen species (ROS) levels, as measured by H_2DCFDA

staining, STM Δ*uppP* displayed only a marginal reduction in viability when subjected to hydrogen peroxide stress (Fig. 2B-C). In contrast, treatment with increasing concentrations of sodium nitrite and peroxynitrite led to significantly decreased viability of STM Δ*uppP* compared to wild-type. (Fig. 2D-G). We evaluated intracellular nitric oxide production in STM Δ*uppP* under sodium nitrite stress using DAF_2DA staining. Flow cytometry-mediated visualisation showed that STM Δ*uppP* demonstrates an increased percentage of DAF_2DA-positive cells upon nitrite stress (Fig. 2H-I). Moreover, on exposure to nitrite stress, STM Δ*uppP* exhibited an elevated median fluorescence intensity (MFI) compared to the wild type, indicating elevated nitric oxide levels (Fig. 2J). Our findings suggest that UppP contributes to *Salmonella* survival in RAW264.7 cells by aiding the bacterial defence against nitrosative stress.

UppP deletion leads to increased nitric oxide (NO) production and nitrotyrosine localisation with intracellular bacteria within macrophages

To evaluate if the reduced fold proliferation of STM Δ*uppP* is attributed to nitrosative stress, we measured nitric oxide production by infected macrophages. We infected RAW 264.7 cells with STM WT and STM Δ*uppP*, transformed with pFPV-mCherry plasmid, responsible for constitutive expression of mCherry [29]. This was followed by DAF_2DA staining 16h post-infection. The STM Δ*uppP*-mCherry infected cells showed increased MFI compared to STM WT-mCherry infected cells, indicating elevated nitric oxide levels (Fig. 3A-B). NO exerts its bactericidal activity by oxidising to form NO adducts, such as nitrites and peroxynitrites, with peroxynitrite nitrosylating tyrosine and impairing protein function [30]. To assess this, we used confocal laser scanning microscopy to estimate nitrotyrosine levels in RAW 264.7 cells 16h post-infection with eGFP-tagged STM WT and STM Δ*uppP*. Our results show that in comparison to STM WT, there is an increase in the colocalisation of nitrotyrosine residues with STM Δ*uppP*. Furthermore, cells infected with STM Δ*uppP* demonstrated increased

levels of nitrotyrosine residues, consistent with our flow cytometry findings (Fig. 3C-E). Additionally, the elevated nitric oxide and nitrotyrosine levels in RAW 264.7 cells infected with STM Δ*uppP* indicate *uppP*'s protective function against nitrosative stress.

UppP mutant shows increased survival on alleviating nitrosative stress

To corroborate our findings of *uppP*'s role in withstanding nitrosative stress, we inhibited inducible nitric oxide synthetase (iNOS) by an irreversible inhibitor, 1400W [19], [31], and observed a rescue in the fold proliferation of STMΔ*uppP* in RAW 264.7 cells (Fig. 4A)

To investigate the role of *uppP* in *Salmonella* pathogenesis *in vivo*, C57BL/6 mice were orally challenged with a dose of 10^7 CFU of STM WT, and STM Δ*uppP* and bacterial burden was assessed 5 days post-infection (Fig. S3A). STM Δ*uppP* displayed reduced dissemination by blood and decreased bacterial loads in the intestine, MLN (mesenteric lymph node), liver and spleen (Fig. S3B-F). Additionally, STM Δ*uppP*-infected mice demonstrated a modest increase in survival compared to STM WT (Fig. S3G). Furthermore, to evaluate if the mutant's attenuation in mice model was due to its increased susceptibility to nitrosative stress, *iNOS*$^{-/-}$ C57BL/6 mice were orally challenged with 10^5 CFU of STM WT and STM Δ*uppP* (Fig. S3H). Notably, STM Δ*uppP* still exhibited attenuation in dissemination and reduced organ burden compared to the wild type (Fig. S3I-M). These findings suggest that UppP may have additional roles in bacterial invasion of intestine, beyond conferring resistance to nitrosative stress To specifically evaluate UppP role in countering nitrosative stress during systemic infection, *iNOS*$^{+/+}$ and *iNOS*$^{-/-}$ C57BL/6 mice were intraperitoneally injected with 10^4 CFU of STM WT and STM Δ*uppP* (Fig. 4C). We observed a significantly increased burden of STM Δ*uppP* in the blood, liver and spleen of *iNOS*$^{-/-}$ mice compared to *iNOS*$^{+/+}$ mice, substantiating the role of UppP in shielding *Salmonella* from nitrosative stress (Fig. 4D-F).

Induction of iNOS and NO production is triggered by downstream signalling from multiple pattern recognition receptors (PRRs). These include but are not limited to TLR4, TLR2, NOD1, and NOD2, out of which the latter of the three receptors detects various components associated with the bacterial peptidoglycan layer [32], [33], [34], [35]. Also, both NOD1 and NOD2 have been reported to localise on *Salmonella*-containing vacuole (SCV) [36], [37]. To evaluate if the enhanced susceptibility of STM Δ*uppP* is due to signalling through NOD receptors, on treatment with RIPK2 inhibitor WEHI-345, we observed a rescue in the fold proliferation of STMΔ*uppP* in RAW 264.7 (Fig. 4B).

Discussion

Cell wall integrity is vital for bacterial structure, protection, and survival. Reports in *Escherichia coli*, *Salmonella* Typhimurium and *Bacillus subtilis* have shown that cell size and shape are affected by changes in growth rate and nutritional availability [38], [39], [40], [41]. Although the STM Δ*uppP* mutant exhibited similar growth rate kinetics to the wild type in LB medium, similar to the observations of *uppP* mutant in *E. coli* [12]. However, we found structural defects in STM Δ*uppP* through SEM and AFM-assisted visualisation. Quantitative analysis of SEM images confirmed a biphasic effect: STM Δ*uppP* cells were shorter in log phase but longer in stationary phase than wild-type cells. This may stem from altered surface area to volume (SA/V) ratios; increased SA/V in log phase could permit division at smaller sizes, while reduced surface area synthesis rate in the stationary phase might affect cell length [42], [43]. Undecaprenyl phosphate is a shared lipid carrier for the peptidoglycan, O antigen and enterobacterial common antigen (ECA) synthesis [22], [23]. Inhibition of either O antigen or ECA synthesis in *E. coli* leads to the accumulation of dead-end undecaprenyl phosphate intermediates, leading to morphological defects [22], [23]. In STM Δ*uppP*,

increased competition for this limited substrate likely alters the stoichiometry between these pathways, leading to the observed morphological changes.

Additionally, the AFM results revealed a reduced Young's modulus of STM Δ*uppP* cells. Drawing a parallel from *E. coli*, where *uppP* accounts for 75% of the undecaprenyl pyrophosphate phosphatase activity [12], combined with our SEM and AFM findings, STM Δ*uppP* may have an altered peptidoglycan organisation. We surmise that the reduced Young's modulus of STMΔ*uppP* may be attributed to changes in the peptidoglycan structure due to the depleted availability of the lipid carrier.

Further to explore the functional consequence of UppP during *Salmonella* pathogenesis, we infected RAW 264.7 murine macrophages and Caco-2 colon carcinoma cells with the STM Δ*uppP*. Though STM Δ*uppP* demonstrated no growth defects in Caco-2, its proliferation was attenuated in RAW 264.7 cells. Resazurin assisted live/ dead assay revealed STM Δ*uppP* had increased susceptibility to nitrosative stress. Moreover, inhibition of inducible nitric oxide synthetase restored the proliferation of STM Δ*uppP* in macrophages. Even though *Salmonella* avoids trafficking of iNOS-containing vesicles to the *Salmonella*-containing vacuole (SCV) in an SPI-2-dependent manner, the freely diffusible nature of NO can facilitate bacterium killing [44], [45]. The altered cell structure of the null mutant may further facilitate NO entry within the bacterium. Also, STMΔ*uppP*-infected macrophages exhibited elevated levels of NO, suggesting the mutant is unable to modulate NO production for survival within macrophages.

The nucleotide oligomerisation domain (NOD) - like receptors 1 and 2 (NOD1/2) are cytoplasmic pattern recognition receptors (PRRs) recognising γ-d-glutamyl-meso-diaminopimelic acid (iE-DAP) and muramyl dipeptide (MDP) which are constituents of the peptidoglycan layer [46]. NOD1 and NOD2, and RIPK2 (downstream effector protein

kinase) are reported to colocalise with the SCV, along with endosomal transporters SLC15A3 and SLC15A4, which translocate MDP to NOD receptors [36], [37]. In the *Salmonella* colitis model, mice deficient for NOD1 and NOD2 have higher bacterial loads in mucosal tissue [47]. *Mycobacterium tuberculosis* growth in human macrophages is controlled by NOD2-dependent NO production [48]. Similarly, NOD2 induces NO, which mediates bacterial clearance in the mouse model of *Chlamydophila pneumoniae*-induced pneumonia [49]. Upon the inhibition of NOD signalling, we observed a rescue in the proliferation of STM Δ*uppP* in macrophages. Undecaprenyl phosphate is a common substrate for synthesising peptidoglycan, O antigen, and ECA, all of which function as essential virulence determinants [50]. Though not explored in our study, there may be an insufficient influx of undecaprenyl phosphate in all the above pathways, leading to the accumulation of precursors and intermediates (especially those of the peptidoglycan synthesis pathways) which may act as ligands to directly or indirectly activate NOD signalling.

In C57BL/6 mice with functional iNOS ($iNOS^{+/+}$), intraperitoneal infection with STM Δ*uppP* showed reduced dissemination by blood and decreased colonisation in the spleen and liver. This phenotype was reversed in iNOS-deficient mice, confirming the role of UppP in promoting *Salmonella* dissemination and colonisation by counteracting nitrosative stress.

To the best of our knowledge, our study is one of the first to report a unique function of undecaprenyl pyrophosphate phosphatase in mitigating nitrosative stress in *Salmonella* (Fig. 5), aside from its canonical roles in cell envelope biogenesis and morphology maintenance. Our findings potentially highlight undecaprenyl phosphate metabolism as a promising target for developing new antimicrobial strategies to enhance the efficacy of macrophage-mediated clearance of *Salmonella* infection.

Material and methods

Bacterial strains and growth condition: *Salmonella enterica* serovar Typhimurium 14028S (STM WT) was used in all experiments. Bacterial strains were cultured in Luria Bertani (LB) broth (HiMedia) with constant shaking (160 rpm) at 37°C (wild type, knockout strains) or 30°C (strains having temperature-sensitive pKD46 plasmid). Ampicillin (50µg/ml), Kanamycin (50µg/ml), Chloramphenicol (25µg/ml) and IPTG (500µM) were used wherever required. A complete list of bacterial strains and plasmids used in this study is provided in Table 1.

Strains/ Plasmids	Characteristics	Source/ Information

Table 1. Strains and plasmids used in this study

Salmonella enterica subspecies *enterica* serovar Typhimurium strain 14028S	Wild type (WT)	Gift from Prof. M. Hensel (Division of Microbiology, University of Osnabrück, Germany)
STMΔ*uppP*	Chl^R	This study
STMΔ*uppP*:pQE60:*uppP*	Chl^R, Amp^R	This study
STM:pFPV-mCherry	Amp^R	Laboratory stock
STMΔ*uppP*:pFPV-mCherry	Chl^R, Amp^R	This study
STM:pFPV25.1	Amp^R	Laboratory stock
STMΔ*uppP*:pFPV25.1	Chl^R, Amp^R	This study
pKD3	Plasmid with FRT flanked by Chloramphenicol-resistance gene, Chl^R	
pKD46	Plasmid expressing λ red recombinase system, Amp^R	
pQE60	Low copy number plasmid, Amp^R	Laboratory stock
pFPV-mCherry	Constitutive expression of mCherry, Amp^R	Laboratory stock
pFPV-GFP	Constitutive expression of GFP, Amp^R	Laboratory stock

Construction of *uppP* knockout strain of *Salmonella*: The knockout strain of *Salmonella* enterica serovar Typhimurium (strain 14028S) was generated using the one-step chromosomal gene inactivation method developed by Datsenko and Wanner [18]. In a concise overview, STM WT was transformed with pKD46 plasmid, housing a 'lambda red recombinase system' controlled by an arabinose-inducible promoter. The transformed cells were cultivated in LB broth with ampicillin (50 μg/mL) and 50 mM arabinose at 30°C until an optical density of 0.35 to 0.4 at 600nm. Electrocompetent STM pKD46 cells were

prepared by washing the bacterial cell pellet thrice with double autoclaved chilled Milli Q water and 10% (v/v) glycerol. Finally, the electrocompetent STM pKD46 cells were resuspended in 50 μL of 10% glycerol. For the knockout procedure, the chloramphenicol-resistant gene cassette (Chl^R, 1.1 kb, used for knocking out *uppP*) was amplified from the pKD3 plasmid, utilising knockout primers. The amplified Chl^R gene cassettes underwent chloroform-isopropanol extraction and were electroporated into STM WT pKD46. The transformed cells were then plated on LB agar with chloramphenicol (25 μg/mL) to select the STM*ΔuppP* strain. Subsequently, the plates were incubated overnight at 37°C. The confirmation of knockout colonies was achieved through expression primers. The primers used for generating the knockout strain are listed in Table 2.

Construction of *uppP* complemented strain of *Salmonella*: The *uppP* gene was amplified using cloning primers through colony PCR. The resulting PCR product, purified via chloroform extraction, was then subjected to BamHI (NEB) and HindIII (NEB) restriction digestion in CutSmart buffer (NEB) at 37°C overnight, alongside the empty pQE60 vector backbone. The double-digested insert and vector were ligated using T4 DNA ligase in 10X ligation buffer (NEB) overnight at 16°C. The ligated product was subsequently transformed into the knockout strains to generate the complemented strain. Verification of complementation was accomplished through the restriction digestion of the recombinant plasmid. The primers used for generating the complement strain are listed in Table 2.

Table 2. List of primer sequences (5’ to 3’)

Primer Name	Sequence (5’ to 3’)
uppP KO FP	CCAAACGGTTATATATGGGGTCTTAACGCGAGATCCATTTCATATGAATATCCTCCTTAG
uppP KO RP	GCCATCCGGCACGGTCAATCATCAGAAGAAGACAACGTAAGTGTAGGCTGGAGCTGCTTC
uppP confirmator	ATTGAGCGTGGCAATAATCTG

y FP	
uppP confirmatory RP	CTGCGCTTATCAGACCGACAA
uppP cloning FP	CGCGGATCCTTGATGAGCGATATGCACTCG
uppP cloning RP	CCCAAGCTTCACGGTCAATCATCAGAAGAA
16S rRNA RT FP	CGCTTCTCTTTGTATGCGCC
16S rRNA RT RP	TCGTCAGCTCGTGTTGTGAA
spiC RT FP	AGGGCCGAAGGTAATAGCCGA
spiC RT RP	CCCATCCGCTGTGAGCTGTA
sifA RT FP	TCGCATCCACAAATGACGGC
sifA RT RP	TTCGCTGCCAGGTAGGTTGC
hilA RT FP	GCCGGTGACCATTACGAAGA
hilA RT RP	AAGAGAGAAGCGGGTTGGTG
sipA RT FP	TTCGGATGAAGCGTTGGTCA
sipA RT RP	GTCATTCGCGTGTGGATTCG
invF RT FP	CGTCGTTTGTGCAGCAGAGC
invF RT RP	TAATTTCCGCGGCGAAACGC
prgH RT FP	CGTTTTCAGGTGTTGCCAGG
prgH RT RP	TACGCGGCTCATCGAAATGA

Growth Curve Analysis: For *in vitro* growth curve experiments, a single colony of each strain was inoculated in Luria Bertani (LB) broth (HiMedia) with constant shaking (160 rpm) at 37°C, with the corresponding antibiotic. Overnight-grown stationary phase bacteria were sub-cultured at a ratio of 1: 100 in freshly prepared LB broth, M9 minimal media and F-media (50mM KCl, 75mM $(NH_4)SO_4$, 5mM K_2SO_4 10mM K_2HPO_4, 1Mm Bis-Tris, 8μM

$MgCl_2$, 38mM glycerol and 0.1% cas amino acids, pH- 5.4) kept at 37ºC, with constant shaking (160 rpm). At different time intervals, aliquots were taken to measure [OD]595nm by TECAN 96 well microplate reader or for CFU analysis.

Scanning electron microscopy (SEM): Logarithmic phase bacterial cultures were drop-casted and immobilised over coverslips by air-drying, followed by overnight fixation with 3.5% glutaraldehyde at 4°C. The following day, the samples were washed with MilliQ water and treated with an increasing ethanol gradient (10%, 30%, 50%, 70%, 90%, and 100%) to facilitate dehydration. The samples were desiccated for 30 minutes, mounted on copper stubs using carbon tape and coated with gold particles under high vacuum. Images were acquired with an ESEM Quanta microscope at a magnification of 5000X. ImageJ was used to analyse bacterial size.

AFM (Atomic force microscopy): Logarithmic phase bacterial cultures were drop-casted and immobilised over coverslips by air-drying, followed by fixation with 3.5% paraformaldehyde. The samples were washed thrice with MilliQ water, followed by desiccation for 30 minutes. Images were acquired from an NX10 AFM. XEI software was utilised to calculate Young's modulus.

Cell culture protocol: DMEM- Dulbecco's Modified Eagle Medium (Lonza) supplemented with 10% FBS (Gibco) was used to culture RAW 264.7 murine macrophages and the human colorectal adenocarcinoma cell line, Caco-2. The cells were maintained at 37°C in a humified incubator with 5% CO_2. Additionally, Caco-2 cells were supplemented with 1% sodium pyruvate (Sigma) and 1% non-essential amino acids (Sigma). Cells were seeded at a density of 1.5 x 10^5 cells per well in a 24-well plate for intracellular survival assay preceding infection.

Gentamicin protection assay: Macrophages or epithelial cells were infected with stationary-phase or logarithmic phase bacterial culture with an MOI of 10. For synchronisation of the infection and enhancing bacterial adhesion, tissue culture plates were centrifugated at 600 rpm for 5 minutes, followed by incubation for 25 minutes at 37°C in a humified incubator with 5% CO_2. Post-incubation cells were washed with 1X PBS, and fresh media (DMEM + 10% FBS) containing 100µg/ml gentamicin was added, followed by 1h of incubation at 37°C and 5% CO_2. Subsequently, the gentamicin concentration was reduced to 25µg/ml and maintained until the cells were harvested.

Percentage phagocytosis and Intracellular proliferation: Following infection of cells with STM at an MOI of 10, cells were treated with DMEM (Sigma) supplemented with 10% FBS (Gibco) containing 100µg/ml gentamicin for 1h. Subsequently, the gentamicin concentration was reduced to 25µg/ml and maintained until the specified time point. Additionally, in some experiments, 1400W dihydrochloride, an inhibitor for inducible nitric oxide synthetase (iNOS), or WEHI-345, a RIPK2 inhibitor which delays NOD signalling [51], is administered to cells at a concentration of 10µM or 1µM, respectively, along with the 25µg/ml gentamicin treatment. 2h and 16h post-infection; cells were lysed in 0.1% triton-X-100. Lysed cells and the pre-inoculum were serially diluted and plated onto LB agar or *Salmonella-Shigella* agar to obtain colony-forming units (CFU). Calculations for percentage phagocytosis and fold proliferation are as follows:

$$Percentage\ Phagocytosis = \frac{No.\ of\ CFU\ at\ 2h}{No.\ of\ CFU\ in\ Pre\ inoculum} \times 100$$

$$Fold\ Proliferation = \frac{No.\ of\ CFU\ at\ 16h}{No.\ of\ CFU\ at\ 2h}$$

RNA isolation and quantitative RT PCR: Bacterial strains were inoculated in LB broth, followed by subculture in LB broth at a ratio of 1:100. Bacterial cells were pelleted and lysed in TRIzol (RNAiso plus Takara). Total RNA was isolated from the TRIzol lysed sample as

per the manufacturer's protocol. Quantification of RNA was performed in NanoDrop (Thermo-Fischer Scientific). The quality of isolated RNA was detected by performing gel electrophoresis with 2% agarose gel. 1μg of RNA was subjected to Turbo DNase (Thermo-Fischer Scientific) treatment at 37°C for 30 minutes, followed by the addition of EDTA and heat inactivation at 65°C for 10 mins. The mRNA was reverse transcribed to cDNA using oligo dT primer, random hexamers, buffer, dNTPs, and reverse transcriptase (Takara) as per the manufacturer's protocol. The expression profile of target genes was evaluated using specific primers by using TB green RT-qPCR master mix (Takara) in the Applied Biosystem QuantStudio-5 system. 16S rRNA was used as an internal control. All the reactions were set up in 384 well plates with three replicates for each sample. The primers used for RT-qPCR are listed in Table 2 [52], [53], [54].

MTT Assay: Post 16h of infection, cells were treated with complete media containing 10μg/ml tetracycline for one hour to kill the intracellular bacteria, to negate the influence of MTT metabolisation by the bacteria [55]. On completion of the tetracycline treatment, fresh incomplete media (i.e. DMEM only) containing 0.5mg/ml MTT (Sigma) was added to cells, followed by 3h of incubation at 37°C and 5% CO2 in the dark. After incubation, media is removed, and DMSO is added, followed by proper aspiration to dissolve the formazan dye. The optical density was measured at 590nm.

Intracellular Reactive oxygen species (ROS) determination using H_2DCFDA staining: Overnight cultures were inoculated into fresh LB media. Upon reaching an optical density of 0.1 (logarithmic phase), H_2DCFDA was added at a final concentration of 10μM to 10^8 CFU/ml of each strain in 1xPBS (pH 7.2) and incubated at 37°C for 30 minutes. Subsequently, 10^7 H_2DCFDA-stained bacterial cells were suspended in 1xPBS (pH 7.2) containing varying concentrations of hydrogen peroxide (1-5mM) and incubated at 37°C with

orbital shaking for 2 hours. The samples were then transferred to a 96-well ELISA plate, and fluorescence was quantified using a Tecan-ELISA plate reader. (Ex-490nm/ Em-520nm).

Bacterial nitric oxide (NO) determination using DAF-2DA staining: The production of nitric oxide (NO) indicates nitrosative stress. We evaluated the NO generation of the strains to *in vitro* nitrite stress by staining with DAF2-DA (4, 5- diamino fluorescein diacetate). DAF2-DA is a cell membrane-permeable dye that forms a membrane-impermeable adduct emitting fluorescence in NO presence. To mimic nitrite stress *in vitro*, 10^8 CFU/ml of bacteria were treated with a range (500μM-5mM) of acidified nitrite (NaNO2 in PBS of pH 5.4) and incubated for 12 hours at 37°C. Post incubation, the cells are treated with 5μM DAF-DA and incubated for 30 minutes at 37°C. BD FACSverse flow cytometer was used to acquire the samples (Ex-491nm/ Em-513nm).

Measurement of NO production in infected macrophages: Intracellular NO production by RAW264.7 cells upon infection was measured by staining with DAF-2DA. 16h post-infection cells were treated with 5μM DAF-2DA and incubated for 30 minutes at 37°C. The cells were washed with 1xPBS and acquired in BD FACSverse flow cytometer (Ex-491nm/ Em-513nm).

Immunofluorescence microscopy for nitrotyrosine residues: RAW264.7 cells were seeded on coverslips and infected with eGFP-tagged strains [56]. The cells were fixed with 3.5% paraformaldehyde (PFA) 16h post-infection. The sample was stained with the rabbit-raised anti-nitrotyrosine antibody (Sigma-Aldrich AB5411) at a dilution of 1:100 (in 2.5% BSA, 0.01% saponin) overnight at 4°C, followed by staining with an anti-rabbit secondary antibody tagged with Cyanine5 (Jackson Laboratory) at a dilution of 1:200 in 2.5% BSA, 0.01% saponin for one hour at room temperature. The coverslips were mounted on glass slides and

sealed with transparent nail polish. The coverslips were imaged by using a Zeiss 880 microscope. Zeiss ZEN Black 2012 software was used to analyse the images.

$$CTCF\ (Corrected\ total\ cell\ fluorescence) = Integrated\ density - (area\ of\ selected\ cell \times mean\ fluorecence\ intensity\ of\ background)$$

Resazurin assay: Resazurin dye was used to evaluate the viability of bacteria when subjected to *in vitro* peroxide stress, acidified nitrite and peroxynitrite stress. 10^8 CFU/ml of bacteria were treated with varying concentrations of H_2O_2 (1-5mM) and acidified nitrite (500µM-5mM), simulating oxidative and nitrosative stress, respectively. For peroxynitrite stress, a combination of H_2O_2 and acidified nitrite was used in a combined concentration range of 62.5µM -1mM. The treated bacteria were incubated for 12 hours at 37°C. On completion of treatment, resazurin was added to the bacteria at a final concentration of 1µg/ml, followed by an incubation at 37°C, for 2 hours. Post incubation, fluorescence intensity was measured in TECAN plate reader (Ex-540nm/ Em-590nm). Percentage viability was calculated by the formula:

$$Percentage\ Viability = \frac{Treated\ Flourescence\ Intensity}{Untreated\ Flourescence\ Intensity} \times 100$$

Bacterial burden in murine model: Specific pathogen-free (SPF) 6-8 weeks old C57BL/6 (*iNOS*$^{+/+}$) and *iNos*$^{-/-}$ (*iNOS* knockout in C57BL/6 background) mice were segregated in cohorts of n=5 or 6. For oral infection, C57BL/6 mice were orally gavaged with 10^7 CFU of STM WT or STM*ΔuppP*. For *iNOS*$^{-/-}$ mice, a dose of 10^5 CFU was administered orally. The infected mice were ethically euthanised 5 days post-infection. For intraperitoneal injection, C57BL/6 (*iNOS*$^{+/+}$) and *iNOS*$^{-/-}$ mice were injected with a dose of 10^4 CFU, followed by ethical euthanasia 3 days post-infection. Bacterial burden was enumerated in the homogenised lysate of organs by serial dilution plating on *Salmonella-Shigella* agar.

Mouse survival assay: Specific pathogen-free (SPF) 6-8 weeks C57BL/6 mice were orally gavaged with 10^7 CFU of STM WT or STM*ΔuppP* (n=6) and monitored daily for mortality. The data is represented as survival percentage.

Statistical analysis: Data was analysed and graphed using the GraphPad Prism 8 software (San Diego, CA). Statistical significance was determined by Student's t-test, One-way ANOVA or Two-way ANOVA to obtain p values. Adjusted p-values below 0.05 are considered statistically significant. The results are expressed as mean ± SD unless mentioned otherwise.

Funding Information

We sincerely appreciate the financial support provided by the Department of Biotechnology (DBT) and the Department of Science and Technology (DST) from the Ministry of Science and Technology. DC acknowledges the Department of Atomic Energy-Scientific Research Council (DAE-SRC) for the Outstanding Investigator Award and funds, ASTRA Chair Professorship, and TATA Innovation fellowship funds. The authors collectively acknowledge the DBT-IISc Partnership Program. We gratefully acknowledge the infrastructure support from the Indian Council of Medical Research (Center for Advanced Study in Molecular Medicine), DST-FIST (Fund for Improvement of Science and Technology Infrastructure), and the University Grants Commission (special assistance). RV acknowledges the Council of Scientific and Industrial Research (CSIR) for fellowship. DM and KP acknowledge the Ministry of Human Resource Development (MHRD) for fellowship. The funders had no role in study design, data collection and analysis, decision to publish, or preparation of the manuscript.

Acknowledgements

We acknowledge the Real-Time Facility, Departmental Confocal Microscopy Facility and Central Instrumentation Facility, at the Department of Microbiology and Cell Biology (MCB), the Division of Biological Sciences Flow Cytometry Facility, the Atomic Force Microscopy (AFM) Facility at the Department of Bioengineering (BE), Advanced Facility for Microscopy and Microanalysis (AFMM) and Central Animal Facility at the Indian Institute of Science (IISc). Mrs. Deepika and Mrs. Monisha are acknowledged for their help in acquiring Scanning Electron Microscopy (SEM) images and AFM images, respectively. We are grateful to Mr. Munish and Mrs. Navya for helping with the data acquisition for flow cytometry. We thank Mr. Arjun Suresh for his assistance with confocal microscopy image acquisition. Dr Abhilash Vijay Nair is acknowledged for providing us with the gene of interest for our study.

Author Contributions

Conceptualisation: RV, DM, KP, and DC; Methodology: RV, DM, KP; Investigation: RV, DM, KP; Data curation: RV, Formal analysis: RV, DM, KP, Fund acquisition: DC, Project administration: RV and DC, Writing-original draft: RV, Editing and proofreading: RV, DM, KP, and DC, Supervision: DC.

References

[1] A. Fàbrega and J. Vila, “Salmonella enterica serovar Typhimurium skills to succeed in the host: Virulence and regulation,” *Clin Microbiol Rev*, vol. 26, no. 2, pp. 308–341, 2013, doi: 10.1128/CMR.00066-12.

[2] R. G. Ferrari, D. K. A. Rosario, A. Cunha-Neto, S. B. Mano, E. E. S. Figueiredo, and C. A. Conte-Juniora, “Worldwide epidemiology of Salmonella serovars in animal-

based foods: A meta-analysis," *Appl Environ Microbiol*, vol. 85, no. 14, Jul. 2019, doi: 10.1128/AEM.00591-19/SUPPL_FILE/AEM.00591-19-S0001.PDF.

[3] S. Issenhuth-Jeanjean *et al.*, "Supplement 2008–2010 (no. 48) to the White–Kauffmann–Le Minor scheme," *Res Microbiol*, vol. 165, no. 7, pp. 526–530, Sep. 2014, doi: 10.1016/J.RESMIC.2014.07.004.

[4] O. Gal-Mor, "Persistent infection and long-term carriage of typhoidal and nontyphoidal salmonellae," *Clin Microbiol Rev*, vol. 32, no. 1, Jan. 2019, doi: 10.1128/CMR.00088-18.

[5] J. D. Stanaway *et al.*, "The global burden of non-typhoidal salmonella invasive disease: a systematic analysis for the Global Burden of Disease Study 2017," *Lancet Infect Dis*, vol. 19, no. 12, pp. 1312–1324, Dec. 2019, doi: 10.1016/S1473-3099(19)30418-9.

[6] "WHO bacterial priority pathogens list, 2024: Bacterial pathogens of public health importance to guide research, development and strategies to prevent and control antimicrobial resistance." Accessed: Apr. 14, 2025. [Online]. Available: https://www.who.int/publications/i/item/9789240093461

[7] WHO, "WHO bacterial priority pathogens list, 2024: Bacterial pathogens of public health importance to guide research, development and strategies to prevent and control antimicrobial resistance," *Bacterial pathogens of public health importance to guide research, development and strategies to prevent and control antimicrobial resistance*, p. 72, 2024, Accessed: Apr. 14, 2025. [Online]. Available: https://www.who.int/publications/i/item/9789240093461

[8] P. Garai, D. P. Gnanadhas, and D. Chakravortty, "Salmonella enterica serovars typhimurium and typhi as model organisms: Revealing paradigm of host-pathogen interactions," *Virulence*, vol. 3, no. 4, pp. 377–388, 2012, doi: 10.4161/viru.21087.

[9] S. Garde, P. K. Chodisetti, and M. Reddy, "Peptidoglycan: Structure, Synthesis, and Regulation," *EcoSal Plus*, vol. 9, no. 2, Dec. 2021, doi: 10.1128/ecosalplus.esp-0010-2020.

[10] G. Manat *et al.*, "Deciphering the metabolism of undecaprenyl-phosphate: The bacterial cell-wall unit carrier at the membrane frontier," in *Microbial Drug Resistance*, Mary Ann Liebert Inc., Jun. 2014, pp. 199–214. doi: 10.1089/mdr.2014.0035.

[11] S. Kumar, A. Mollo, D. Kahne, and N. Ruiz, "The Bacterial Cell Wall: From Lipid II Flipping to Polymerization," *Chem Rev*, vol. 122, no. 9, pp. 8884–8910, May 2022, doi: 10.1021/ACS.CHEMREV.1C00773/ASSET/IMAGES/LARGE/CR1C00773_0011.JPEG.

[12] M. El Ghachi, A. Bouhss, D. Blanot, and D. Mengin-Lecreulx, “The bacA gene of Escherichia coli encodes an undecaprenyl pyrophosphate phosphatase activity,” *Journal of Biological Chemistry*, vol. 279, no. 29, pp. 30106–30113, Jul. 2004, doi: 10.1074/jbc.M401701200.

[13] S. D. Workman and N. C. J. Strynadka, “A Slippery Scaffold: Synthesis and Recycling of the Bacterial Cell Wall Carrier Lipid,” *J Mol Biol*, vol. 432, no. 18, pp. 4964–4982, Aug. 2020, doi: 10.1016/J.JMB.2020.03.025.

[14] B. D. Cain, P. J. Norton, W. Eubanks, H. S. Nick, and C. M. Allen, “Amplification of the bacA Gene Confers Bacitracin Resistance to Escherichia coli,” 1993.

[15] A. F. Chalker *et al.*, “The bacA gene, which determines bacitracin susceptibility in Streptococcus pneumoniae and Staphylococcus aureus, is also required for virulence,” 2000. [Online]. Available: www.tigr.org

[16] L. Röse, S. H. E. Kaufmann, and S. Daugelat, “Involvement of Mycobacterium smegmatis undecaprenyl phosphokinase in biofilm and smegma formation,” *Microbes Infect*, vol. 6, no. 11, pp. 965–971, Sep. 2004, doi: 10.1016/J.MICINF.2004.05.011.

[17] S. B. Hernández *et al.*, “Peptidoglycan editing in non-proliferating intracellular Salmonella as source of interference with immune signaling,” *PLoS Pathog*, vol. 18, no. 1, p. e1010241, Jan. 2022, doi: 10.1371/JOURNAL.PPAT.1010241.

[18] K. A. Datsenko and B. L. Wanner, “One-step inactivation of chromosomal genes in Escherichia coli K-12 using PCR products,” *Proc Natl Acad Sci U S A*, vol. 97, no. 12, pp. 6640–6645, Jun. 2000, doi: 10.1073/PNAS.120163297/ASSET/103C1B8D-D302-4337-8E67-9F9084156407/ASSETS/GRAPHIC/PQ1201632006.JPEG.

[19] A. R. Chowdhury, S. Sah, U. Varshney, and D. Chakravortty, “Salmonella Typhimurium outer membrane protein A (OmpA) renders protection from nitrosative stress of macrophages by maintaining the stability of bacterial outer membrane,” *PLoS Pathog*, vol. 18, no. 8, p. e1010708, Aug. 2022, doi: 10.1371/JOURNAL.PPAT.1010708.

[20] J. Delwick, T. Nikolaus, S. Erdogan, and M. Hensel, “Environmental regulation of Salmonella pathogenicity island 2 gene expression,” *Mol Microbiol*, vol. 31, no. 6, pp. 1759–1773, Apr. 1999, doi: 10.1046/J.1365-2958.1999.01312.X.

[21] M. A. Jorgenson and J. C. Bryant, “A genetic screen to identify factors affected by undecaprenyl phosphate recycling uncovers novel connections to morphogenesis in Escherichia coli,” *Mol Microbiol*, vol. 115, no. 2, pp. 191–207, Feb. 2021, doi: 10.1111/mmi.14609.

[22] M. A. Jorgenson, S. Kannan, M. E. Laubacher, and K. D. Young, “Dead-end intermediates in the enterobacterial common antigen pathway induce morphological defects in Escherichia coli by competing for undecaprenyl phosphate,” *Mol Microbiol*, vol. 100, no. 1, pp. 1–14, Apr. 2016, doi: 10.1111/mmi.13284.

[23] M. A. Jorgenson and K. D. Young, “Interrupting biosynthesis of O antigen or the lipopolysaccharide core produces morphological defects in Escherichia coli by sequestering undecaprenyl phosphate,” *J Bacteriol*, vol. 198, no. 22, pp. 3070–3079, 2016, doi: 10.1128/JB.00550-16.

[24] G. Wood *et al.*, “Salmonella injectisome penetration of macrophages triggers rapid translation of transcription factors and protection against cell death,” *bioRxiv*, p. 2023.07.21.550113, Jul. 2024, doi: 10.1101/2023.07.21.550113.

[25] D. Hersh, D. M. Monack, M. R. Smith, N. Ghori, S. Falkow, and A. Zychlinsky, “The Salmonella invasin SipB induces macrophage apoptosis by binding to caspase-1,” *Proc Natl Acad Sci U S A*, vol. 96, no. 5, pp. 2396–2401, Mar. 1999, doi: 10.1073/PNAS.96.5.2396/ASSET/F6D52141-9395-4E16-A419-3F95A9B47CA4/ASSETS/GRAPHIC/PQ0494845006.JPEG.

[26] Y. Zhang *et al.*, “Programmed cell death and Salmonella pathogenesis: an interactive overview,” *Front Microbiol*, vol. 14, p. 1333500, Jan. 2023, doi: 10.3389/FMICB.2023.1333500/BIBTEX.

[27] A. McIntosh *et al.*, “SipA activation of caspase-3 is a decisive mediator of host cell survival at early stages of Salmonella enterica serovar Typhimurium infection,” *Infect Immun*, vol. 85, no. 9, Sep. 2017, doi: 10.1128/IAI.00393-17/SUPPL_FILE/ZII999092114SM5.AVI.

[28] E. Jennings, T. L. M. Thurston, and D. W. Holden, “Salmonella SPI-2 Type III Secretion System Effectors: Molecular Mechanisms And Physiological Consequences,” *Cell Host Microbe*, vol. 22, no. 2, pp. 217–231, 2017, doi: 10.1016/j.chom.2017.07.009.

[29] D. Drecktrah *et al.*, “Dynamic Behavior of Salmonella-Induced Membrane Tubules in Epithelial Cells,” *Traffic*, vol. 9, no. 12, pp. 2117–2129, Dec. 2008, doi: 10.1111/J.1600-0854.2008.00830.X.

[30] C. A. Henard and A. Vázquez-Torres, “Nitric oxide and salmonella pathogenesis,” *Front Microbiol*, vol. 2, no. APR, p. 9906, Apr. 2011, doi: 10.3389/FMICB.2011.00084/BIBTEX.

[31] E. P. Garvey *et al.*, “1400W Is a Slow, Tight Binding, and Highly Selective Inhibitor of Inducible Nitric-oxide Synthase in Vitro and in Vivo,” *Journal of Biological Chemistry*, vol. 272, no. 8, pp. 4959–4963, Feb. 1997, doi: 10.1074/JBC.272.8.4959.

[32] S. Mukherjee, S. Karmakar, and S. P. S. Babu, “TLR2 and TLR4 mediated host immune responses in major infectious diseases: a review,” *The Brazilian Journal of Infectious Diseases*, vol. 20, no. 2, pp. 193–204, Mar. 2016, doi: 10.1016/J.BJID.2015.10.011.

[33] L. O. Moreira and D. S. Zamboni, “NOD1 and NOD2 signaling in infection and inflammation,” *Front Immunol*, vol. 3, no. NOV, p. 35118, Nov. 2012, doi: 10.3389/FIMMU.2012.00328/XML/NLM.

[34] S. To□temeyer *et al.*, “IFN-γ Enhances Production of Nitric Oxide from Macrophages via a Mechanism That Depends on Nucleotide Oligomerization Domain-2,” *The Journal of Immunology*, vol. 176, no. 8, pp. 4804–4810, Apr. 2006, doi: 10.4049/JIMMUNOL.176.8.4804.

[35] S. Thoma-Uszynski *et al.*, “Induction of direct antimicrobial activity through mammalian toll-like receptors,” *Science (1979)*, vol. 291, no. 5508, pp. 1544–1547, Feb. 2001, doi: 10.1126/SCIENCE.291.5508.1544/ASSET/AF8C5909-6776-4874-9ADC-0D81695FA094/ASSETS/GRAPHIC/SE0619197003.JPEG.

[36] Y. Lu *et al.*, “Palmitoylation of NOD1 and NOD2 is required for bacterial sensing,” *Science (1979)*, vol. 366, no. 6464, pp. 460–467, Oct. 2019, doi: 10.1126/SCIENCE.AAU6391/SUPPL_FILE/AAU6391-LU-SM.PDF.

[37] N. Nakamura *et al.*, “Endosomes are specialised platforms for bacterial sensing and NOD2 signalling,” *Nature 2014 509:7499*, vol. 509, no. 7499, pp. 240–244, Mar. 2014, doi: 10.1038/nature13133.

[38] M. Schaechter, O. MaalØe, and N. O. Kjeldgaard, “Dependency on Medium and Temperature of Cell Size and Chemical Composition during Balanced Growth of Salmonella typhimurium,” *Microbiology (N Y)*, vol. 19, no. 3, pp. 592–606, Dec. 1958, doi: 10.1099/00221287-19-3-592.

[39] H. Bremer and P. P. Dennis, “Modulation of Chemical Composition and Other Parameters of the Cell at Different Exponential Growth Rates,” *EcoSal Plus*, vol. 3, no. 1, Jan. 2008, doi: 10.1128/ECOSAL.5.2.3/ASSET/EC65E8C7-8572-4870-BAE2-75BD45F44790/ASSETS/GRAPHIC/FIG3.GIF.

[40] M. G. Sargent, “Control of cell length in Bacillus subtilis,” *J Bacteriol*, vol. 123, no. 1, pp. 7–19, Jul. 1975, doi: 10.1128/JB.123.1.7-19.1975.

[41] S. Vadia and P. A. Levin, “Growth rate and cell size: a re-examination of the growth law,” *Curr Opin Microbiol*, vol. 24, pp. 96–103, Apr. 2015, doi: 10.1016/J.MIB.2015.01.011.

[42] L. K. Harris and J. A. Theriot, “Surface Area to Volume Ratio: A Natural Variable for Bacterial Morphogenesis,” *Trends Microbiol*, vol. 26, no. 10, pp. 815–832, Oct. 2018, doi: 10.1016/J.TIM.2018.04.008.

[43] L. K. Harris and J. A. Theriot, “Relative Rates of Surface and Volume Synthesis Set Bacterial Cell Size,” *Cell*, vol. 165, no. 6, pp. 1479–1492, Jun. 2016, doi: 10.1016/J.CELL.2016.05.045.

[44] D. Chakravortty, I. Hansen-Wester, and M. Hensel, “Salmonella pathogenicity island 2 mediates protection of intracellular Salmonella from reactive nitrogen intermediates,”

Journal of Experimental Medicine, vol. 195, no. 9, pp. 1155–1166, 2002, doi: 10.1084/jem.20011547.

[45] D. Chakravortty and M. Hensel, “Inducible nitric oxide synthase and control of intracellular bacterial pathogens,” *Microbes Infect*, vol. 5, no. 7, pp. 621–627, Jun. 2003, doi: 10.1016/S1286-4579(03)00096-0.

[46] D. J. Philpott, M. T. Sorbara, S. J. Robertson, K. Croitoru, and S. E. Girardin, “NOD proteins: regulators of inflammation in health and disease,” *Nature Reviews Immunology 2013 14:1*, vol. 14, no. 1, pp. 9–23, Dec. 2013, doi: 10.1038/nri3565.

[47] K. Geddes *et al.*, “Nod1 and Nod2 regulation of inflammation in the Salmonella colitis model,” *Infect Immun*, vol. 78, no. 12, pp. 5107–5115, Dec. 2010, doi: 10.1128/IAI.00759-10/SUPPL_FILE/NOD_PATH_PAPER_SUP_3_2.ZIP.

[48] M. B. Landes, † Murugesan, V. S. Rajaram, H. Nguyen, and L. S. Schlesinger, “Role for NOD2 in Mycobacterium tuberculosis-induced iNOS expression and NO production in human macrophages,” *J Leukoc Biol*, vol. 97, no. 6, pp. 1111–1119, Jun. 2015, doi: 10.1189/JLB.3A1114-557R.

[49] K. Shimada *et al.*, “The NOD/RIP2 Pathway Is Essential for Host Defenses Against Chlamydophila pneumoniae Lung Infection,” *PLoS Pathog*, vol. 5, no. 4, p. e1000379, Apr. 2009, doi: 10.1371/JOURNAL.PPAT.1000379.

[50] L. D. Tatar, C. L. Marolda, A. N. Polischuk, D. van Leeuwen, and M. A. Valvano, “An Escherichia coli undecaprenyl-pyrophosphate phosphatase implicated in undecaprenyl phosphate recycling,” *Microbiology (N Y)*, vol. 153, no. 8, pp. 2518–2529, Aug. 2007, doi: 10.1099/mic.0.2007/006312-0.

[51] U. Nachbur *et al.*, “A RIPK2 inhibitor delays NOD signalling events yet prevents inflammatory cytokine production,” *Nature Communications 2015 6:1*, vol. 6, no. 1, pp. 1–13, Mar. 2015, doi: 10.1038/ncomms7442.

[52] A. Datey *et al.*, “Rewiring of one carbon metabolism in Salmonella serves as an excellent live vaccine against systemic salmonellosis,” *Vaccine*, vol. 36, no. 50, pp. 7715–7727, Nov. 2018, doi: 10.1016/J.VACCINE.2018.10.079.

[53] A. V. Nair, A. Singh, R. S. Rajmani, and D. Chakravortty, “Salmonella Typhimurium employs spermidine to exert protection against ROS-mediated cytotoxicity and rewires host polyamine metabolism to ameliorate its survival in macrophages,” *Redox Biol*, vol. 72, p. 103151, Jun. 2024, doi: 10.1016/J.REDOX.2024.103151.

[54] D. Mukherjee and D. Chakravortty, “A Tale of Twins: The Distinct Roles of Intracellular and Extracellular Formate in Regulating Flagellar and Pathogenicity Island-1 Genes in Salmonella Typhimurium,” *bioRxiv*, p. 2024.01.30.577997, Nov. 2024, doi: 10.1101/2024.01.30.577997.

[55] S. Grille *et al.*, “Salmonella enterica serovar Typhimurium immunotherapy for B-cell lymphoma induces broad anti-tumour immunity with therapeutic effect,” *Immunology*, vol. 143, no. 3, pp. 428–437, Nov. 2014, doi: 10.1111/IMM.12320.

[56] R. H. Valdivia, A. E. Hromockyj, D. Monack, L. Ramakrishnan, and S. Falkow, “Applications for green fluorescent protein (GFP) in the study of hostpathogen interactions,” *Gene*, vol. 173, no. 1, pp. 47–52, Jan. 1996, doi: 10.1016/0378-1119(95)00706-7.

Main Figures

Figure 1

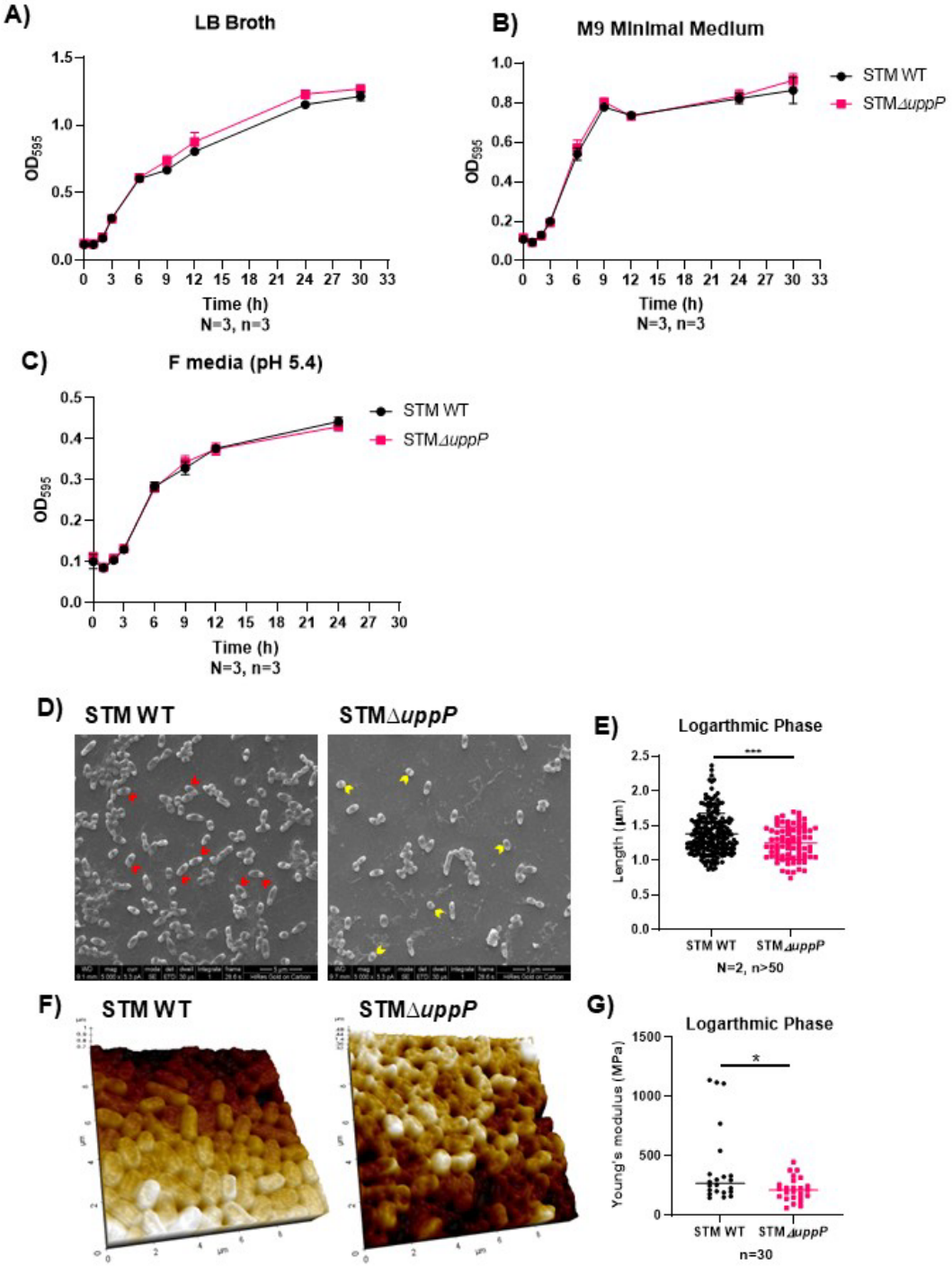
A)
LB Broth
OD595
Time (h)
N=3, n=3
B)
M9 Minimal Medium
STM WT
STMΔuppP
OD595
Time (h)
N=3, n=3
C)
F media (pH 5.4)
STM WT
STMΔuppP
OD595
Time (h)
N=3, n=3
D)
STM WT
STMΔuppP
E)
Logarthmic Phase
Length (µm)
STM WT
STMΔuppP
N=2, n>50
F)
STM WT
STMΔuppP
G)
Logarthmic Phase
Young's modulus (MPa)
STM WT
STMΔuppP
n=30

642

Figure 1. Loss of *uppP* affects the bacterial cell dimensions and strength

A-C) Growth kinetics of STM WT and STM Δ*uppP* by measuring optical density at 595nm (OD_{595}) in LB (Luria Bertani) broth (A), M9 minimal media (B), and acidic F-media (C). Data are representative of N=3, n=3 ± SD (standard deviation).

D) Representative scanning electron micrographs of STM WT and STM Δ*uppP* logarithmic phase cells. Red and yellow arrows represent cells with increased and decreased length, respectively. Scale bar = 5μm

E) Quantification of the length of the bacterial cells captured in the SEM images. Data are representative of N=2, n≥50 ± SD (standard deviation). Unpaired two-tailed Student's t-test was performed to obtain the p values. (***P<0.0005, **P<0.001, *P<0.05, ns- non-significant)

F) Representative atomic force micrographs of STM WT and STM Δ*uppP*. A 20 x 20μm^2 area from each coverslip was selected for imaging.

G) Quantification of Young's modulus of the bacterial cells captured in the AFM images. Data are representative of n≥30 ± SD (standard deviation). Unpaired two-tailed Student's t-test was performed to obtain the p values. (***P<0.0005, **P<0.001, *P<0.05, ns- non-significant)

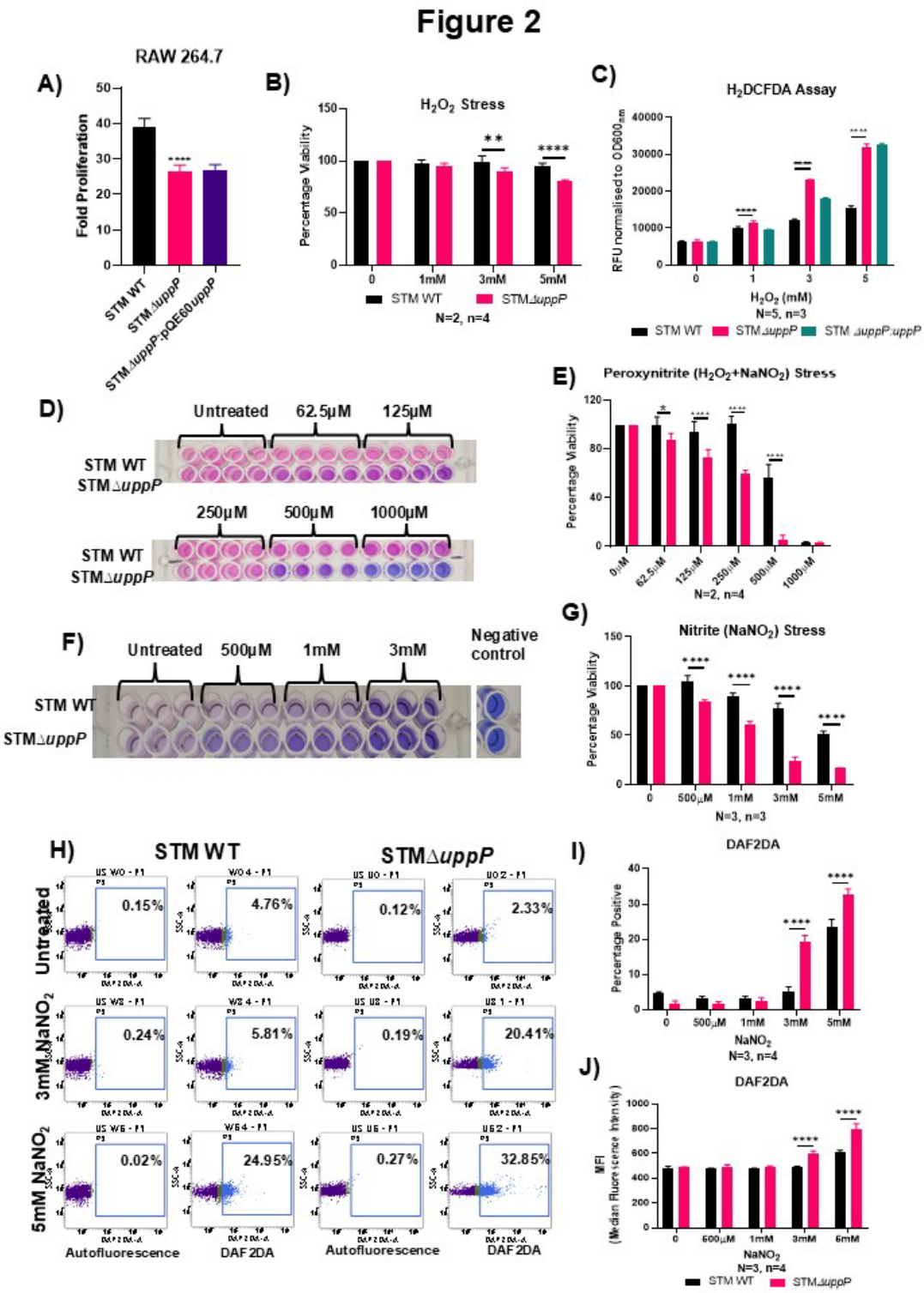

Figure 2. *uppP* facilitates *Salmonella* to withstand nitrite and peroxynitrite stress

A) Fold proliferation of STM WT, STM Δ*uppP*, and STM Δ*uppP*:pQE60-*uppP*, within RAW 264.7 macrophages (MOI=10). Results are mean of N=3, n=3 ± SEM (standard error of

mean). An unpaired two-tailed student's t-test was performed to obtain the p values. (****P<0.0001, ***P<0.0005, **P<0.001, *P<0.05, ns- non-significant)

B) Percentage viability of STM WT and STM *ΔuppP* in the presence of varying concentrations of H_2O_2 measured by resazurin assay. Results are representative of N=2, n=4 ± SD. Two-way ANOVA was performed to obtain the p values. (****P<0.0001, ***P<0.0005, **P<0.001, *P<0.05, ns- non-significant).

C) Estimation of reactive oxygen species (ROS) levels in STM WT and STM *ΔuppP* by H_2DCFDA staining in the presence of varying concentrations of H_2O_2. Results are representative of N=5, n=4 ± SD. Two-way ANOVA was performed to obtain the p values. (****P<0.0001, ***P<0.0005, **P<0.001, *P<0.05, ns- non-significant).

D-E) Percentage viability (D) and representative image (E) of resazurin assay of STM WT and STM *ΔuppP* in the presence of varying concentrations of $NaNO_2$ (*in vitro* nitrite stress). Results are representative of N=3, n=3 ± SD. Two-way ANOVA was performed to obtain the p-values. (****P<0.0001, ***P<0.0005, **P<0.001, *P<0.05, ns- non-significant).

F-G) Percentage viability (F) and representative images (G) of resazurin assay of STM WT and STM *ΔuppP* in the presence of varying concentrations of $NaNO_2$ + H_2O_2 (*in vitro* peroxynitrite stress). Results are representative of N=2, n=4 ± SD. Two-way ANOVA was performed to obtain the p values. (****P<0.0001, ***P<0.0005, **P<0.001, *P<0.05, ns- non-significant).

H-J) Estimation of nitric oxide in STM WT and STM *ΔuppP* by DAF_2DA staining in the presence of varying concentrations of $NaNO_2$ by flow cytometry. Representative SSCA vs DAF_2DA dot plots of STM WT and STM *ΔuppP* (H). Quantification of DAF2DA positive percentage population (I) and median fluorescence intensity (MFI) (J). Results are

representative of N=3, n=4 ± SD. Two-way ANOVA was performed to obtain the p values. (****P<0.0001, ***P<0.0005, **P<0.001, *P<0.05, ns- non-significant).

Figure 3

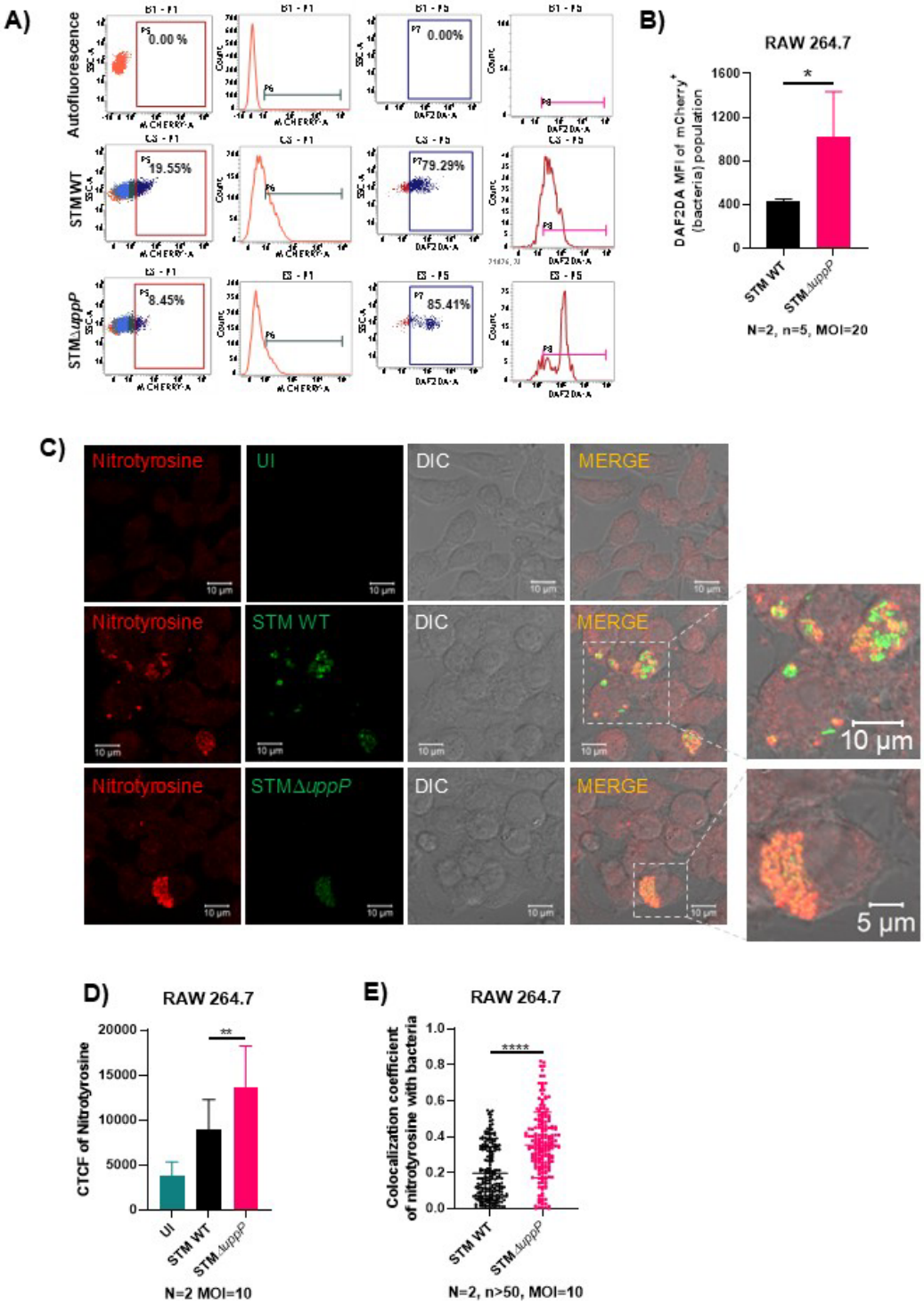
A)
Autofluorescence
STM WT
STMΔuppP
0.00 %
0.00%
19.55%
79.29%
8.45%
85.41%
B)
RAW 264.7
DAF2DA MFI of mCherry+ (bacteria) population
STM WT
STMΔuppP
N=2, n=5, MOI=20
C)
Nitrotyrosine
UI
DIC
MERGE
STM WT
STMΔuppP
10 µm
5 µm
D)
RAW 264.7
CTCF of Nitrotyrosine
UI
STM WT
STMΔuppP
N=2 MOI=10
E)
RAW 264.7
Colocalization coefficient of nitrotyrosine with bacteria
STM WT
STMΔuppP
N=2, n>50, MOI=10

688

Figure 3. *uppP* sustains *Salmonella* survival in macrophages by countering host-induced nitrosative stress

A-B) Estimation of nitric oxide in macrophages infected with mCherry-tagged STM WT and STM *ΔuppP* by DAF_2DA staining followed by flow cytometry. Representative mCherry vs SSC-A, DAF_2DA vs SSC-A, dot plots and histograms of STM WT and STM *ΔuppP* (A). Quantification of DAF_2DA median fluorescence intensity (MFI) of the mCherry-positive population (B). Results are representative of N=2, n=4 ± SD. An unpaired two-tailed Student's t-test was performed to obtain the p-values. (****P<0.0001, ***P<0.0005, **P<0.001, *P<0.05, ns- non-significant).

C-E) Representative immunofluorescence images of RAW 264.7 cells infected with STM WT and STM Δ*uppP* for 16h, MOI=10 (C). Quantification of colocalisation of nitrotyrosine with bacteria (D) and corrected total cell fluorescence (CTCF) of nitrotyrosine in infected cells (E). Results are representative of N=2, n≥50 ± SD. Unpaired two-tailed Student's t-test was performed to obtain the p values. (****P<0.0001, ***P<0.0005, **P<0.001, *P<0.05, ns-non-significant).

Figure 4

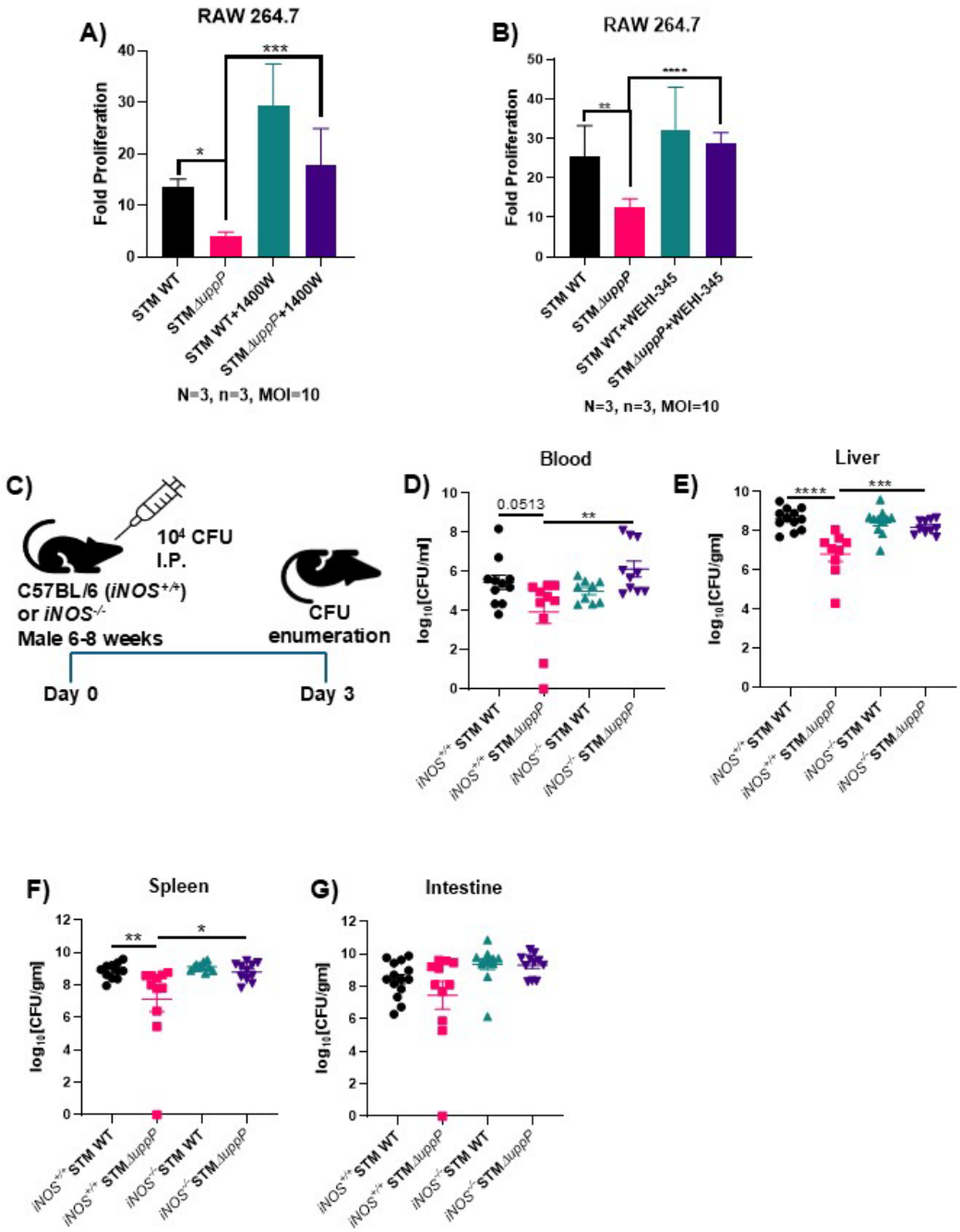

Figure 4. *uppP* counters nitrosative stress during systemic infection

A-B) Fold proliferation of STM WT and STM Δ*uppP* within RAW 264.7 macrophages on treatment with 1400W (A) or WEHI-345 (B) MOI=10. Results are representative of N=3,

n=3 ± SD (standard deviation). One-way ANOVA was performed to obtain the p-values. (****P<0.0001, ***P<0.0005, **P<0.001, *P<0.05, ns- non-significant).

C) Schematic representation of the experimental protocol followed for intraperitoneal (I.P.) and infection enumerating bacterial burden in tissues

D-G) Enumeration of bacterial burden in the blood (D), liver (E), spleen (F) and intestine (G) on infection via intraperitoneal injection in C57BL/6 (*iNOS*$^{+/+}$) and *iNOS*$^{-/-}$ mice. Results are representative of N=2 n=6 ± SEM (standard deviation). Mann-Whitney test was performed to obtain the p values. (****P<0.0001, ***P<0.0005, **P<0.001, *P<0.05, ns- non-significant).

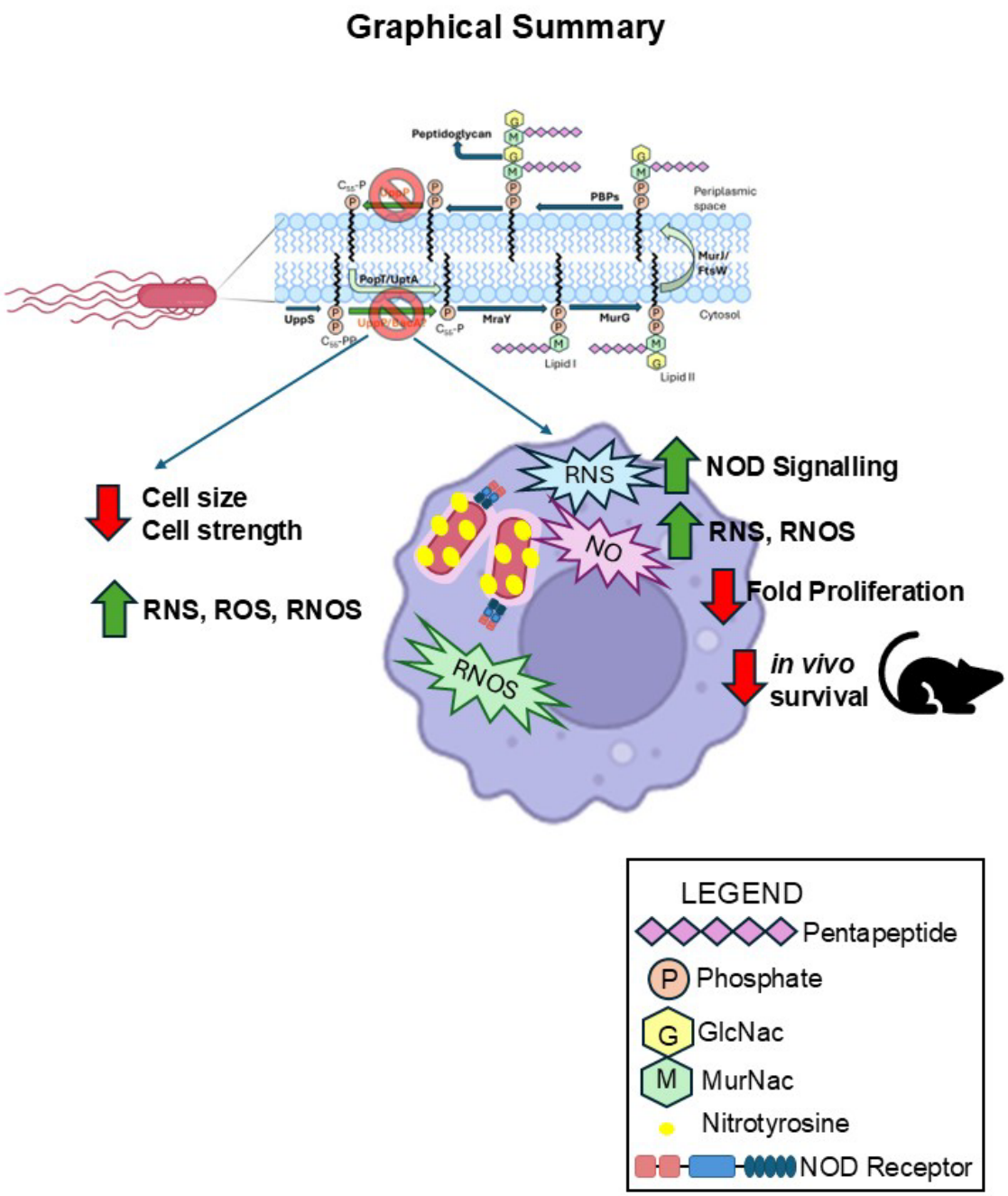

Figure 5. Graphical Abstract

Increased susceptibility of STM Δ*uppP* to host nitrosative stress is indicated by elevated NO levels in RAW 264.7 cells and a greater accumulation of nitrotyrosine residues on the mutant. The elevated NO levels may be due to activation of NOD receptors, which is one of the factors contributing to STM Δ*uppP*'s reduced fold proliferation in RAW 264.7 cells and

attenuated survival in the mouse model. NO: Nitric oxide, RNS: reactive nitrogen species, RNOS: Reactive Nitrogen Oxygen Species, NOD: Nucleotide-binding oligomerisation domain-containing protein, GlcNac: N-acetylglucosamine, MurNac: N-Acetylmuramic acid.

Figure S1

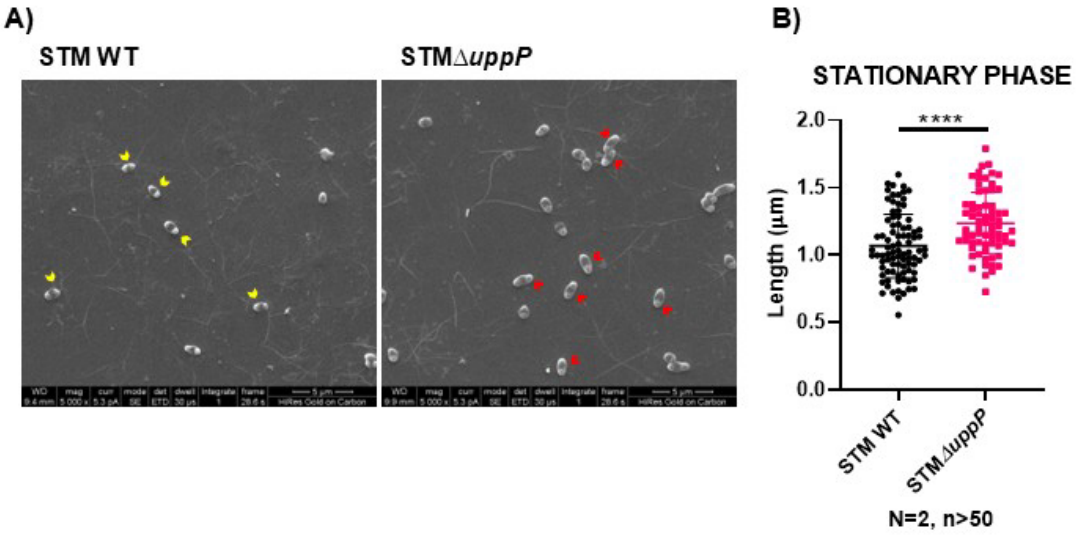

Supplementary Figures

Figure S1. Loss of *uppP* affects the bacterial cell dimensions in the stationary phase

A) Representative scanning electron micrographs of STM WT and STM Δ*uppP* stationary phase cells. Red and yellow arrows represent cells with increased and decreased length, respectively. Scale bar = 5µm

B) Quantification of the length of the bacterial cells captured in the SEM images. Data are representative of N=2, n≥50 ± SD (standard deviation). Unpaired two-tailed Student's t-test was performed to obtain the p values. (***P<0.0005, **P<0.001, *P<0.05, ns- non-significant)

Figure S2

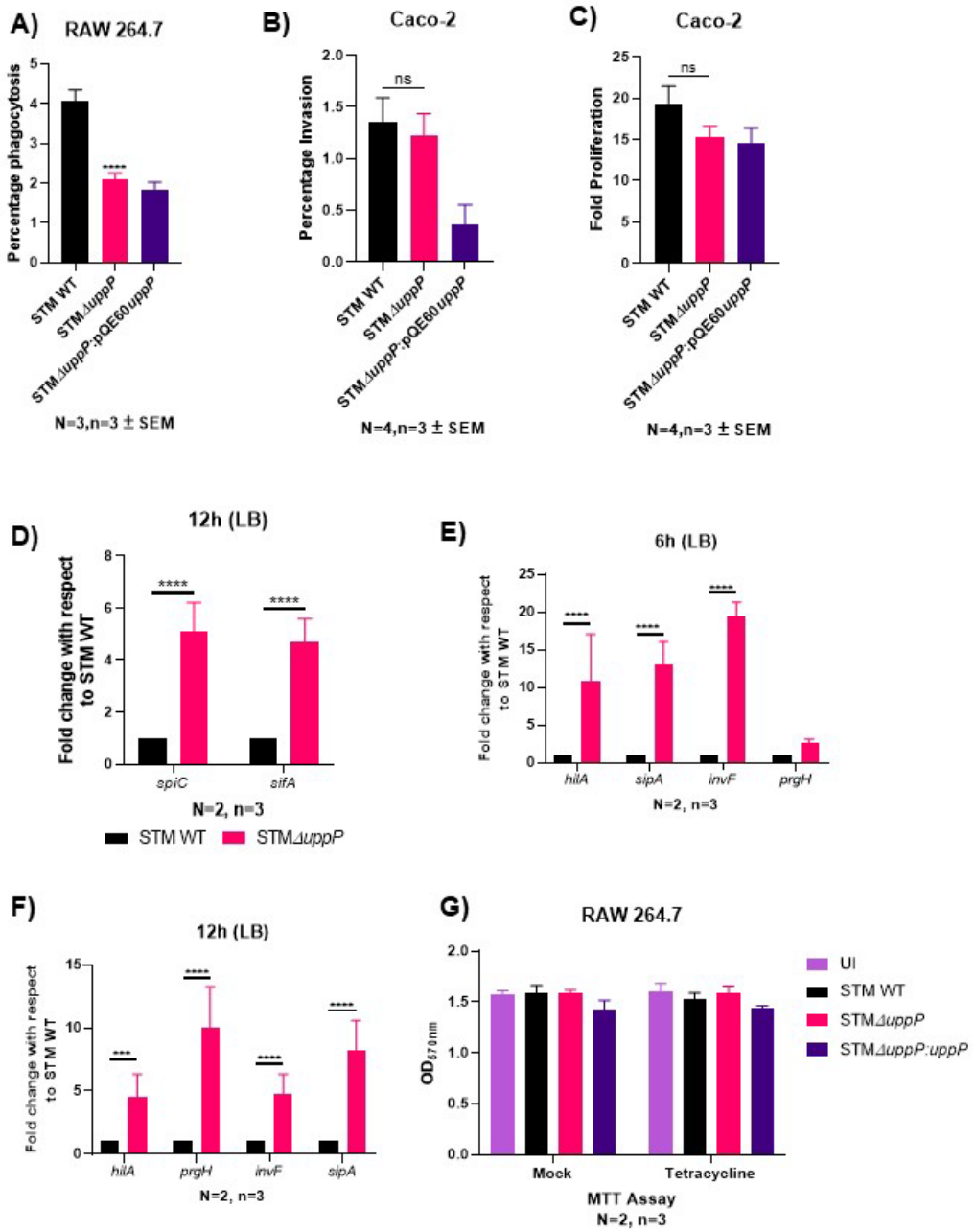

Figure S2. *uppP* facilitates intracellular survival of *Salmonella* in macrophages

A) Percentage phagocytosis of STM WT, STM Δ*uppP*, and STM Δ*uppP*:pQE60-*uppP*, within RAW 264.7 macrophages (MOI=10). Results are mean of N=3, n=3 ± SEM (standard error of mean). An unpaired two-tailed student's t-test was performed to obtain the p values. (****P<0.0001, ***P<0.0005, **P<0.001, *P<0.05, ns- non-significant)

B-C) Percentage invasion (B) and fold proliferation (C) of STM WT, STM Δ*uppP* and STM Δ*uppP*:pQE60-*uppP* within colorectal adenocarcinoma cell line-Caco-2 (MOI=10). Results are mean of N=3, n=3 ± SEM (standard error of mean). An unpaired two-tailed student's t-test was performed to obtain the p values. (****P<0.0001, ***P<0.0005, **P<0.001, *P<0.05, ns- non-significant)

D-E) Quantification of the expression of *hilA*, *prgH*, *invF* and *sipA* during logarithmic (E) and stationary (F) phase in STM WT and STM *ΔuppP* cultured in LB broth. Results are representative of N=2, n=3 ± SD. Two-way ANOVA was performed to obtain the p values. (****P<0.0001, ***P<0.0005, **P<0.001, *P<0.05, ns- non-significant).

F) Cell viability assay of RAW 264.7 cells, 16h post-infection with STM WT, STM Δ*uppP*, and STM Δ*uppP*:pQE60-*uppP*. Results are representative of N=2, n=3 ± SD. Two-way ANOVA was performed to obtain the p values. (****P<0.0001, ***P<0.0005, **P<0.001, *P<0.05, ns- non-significant).

G) Quantification of the expression of *spiC* and *sifA* during the stationary phase in STM WT and STM *ΔuppP* cultured in LB broth. Results are representative of N=2, n=3 ± SD. Two-way ANOVA was performed to obtain the p values. (****P<0.0001, ***P<0.0005, **P<0.001, *P<0.05, ns- non-significant).

Figure S3

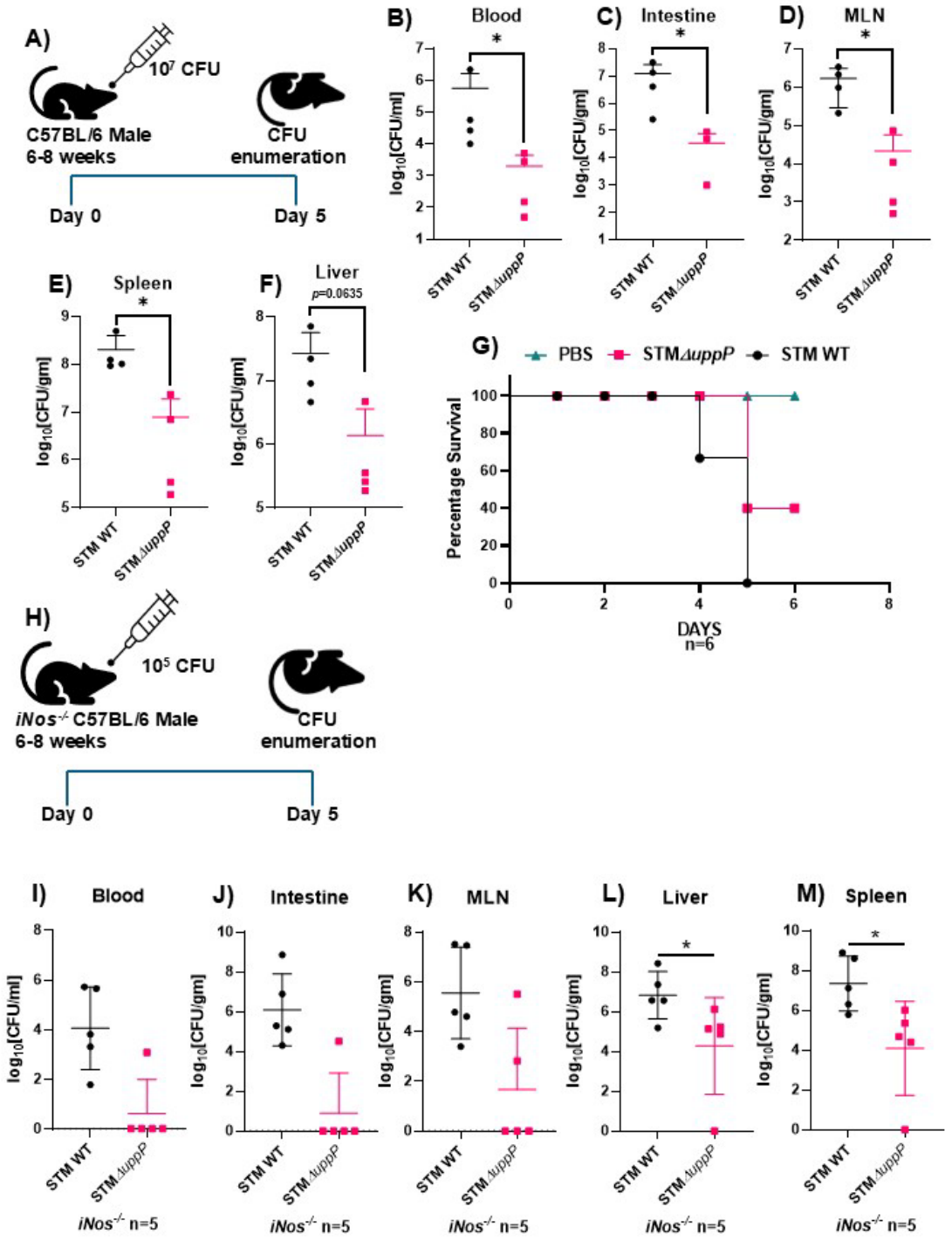
A)
10⁷ CFU
C57BL/6 Male
6-8 weeks
CFU
enumeration
Day 0
Day 5
B) Blood
C) Intestine
D) MLN
log10[CFU/ml]
log10[CFU/gm]
STM WT
STMΔuppP
E) Spleen
F) Liver
p=0.0635
G)
PBS
STMΔuppP
STM WT
Percentage Survival
DAYS
n=6
H)
10⁵ CFU
iNos-/- C57BL/6 Male
6-8 weeks
CFU
enumeration
Day 0
Day 5
I) Blood
J) Intestine
K) MLN
L) Liver
M) Spleen
iNos-/- n=5

Figure S3. UppP facilitates *Salmonella* survival in the *in vivo* murine model

A) Schematic representation of the experimental protocol followed for enumerating bacterial burden in tissues upon oral gavage in C57BL/6 ($iNOS^{+/+}$) mice.

B-F) Enumeration of bacterial burden in the blood (B), intestine (C), MLN (D), spleen (E) and liver (F) on infection via oral route in C57BL/6 ($iNOS^{+/+}$) mice. Results are representative of N=2, n=6 ± SD (standard deviation). Mann-Whitney test was performed to obtain the p-values. (****P<0.0001, ***P<0.0005, **P<0.001, *P<0.05, ns- non-significant).

G) Percentage survival of C57BL/6 ($iNOS^{+/+}$) mice infected with STM WT and STMΔ*uppP* via the oral route.

H) Schematic representation of the experimental protocol followed for enumerating bacterial burden in tissues upon oral gavage in $iNOS^{-/-}$ mice.

I-M) Enumeration of bacterial burden in the blood (I), intestine (J), MLN (K), liver (L) and spleen (M) on infection via oral route in $iNOS^{-/-}$ mice. Results are representative of n=5 ± SD (standard deviation). Mann-Whitney test was performed to obtain the p values. (****P<0.0001, ***P<0.0005, **P<0.001, *P<0.05, ns- non-significant).

Figure S4

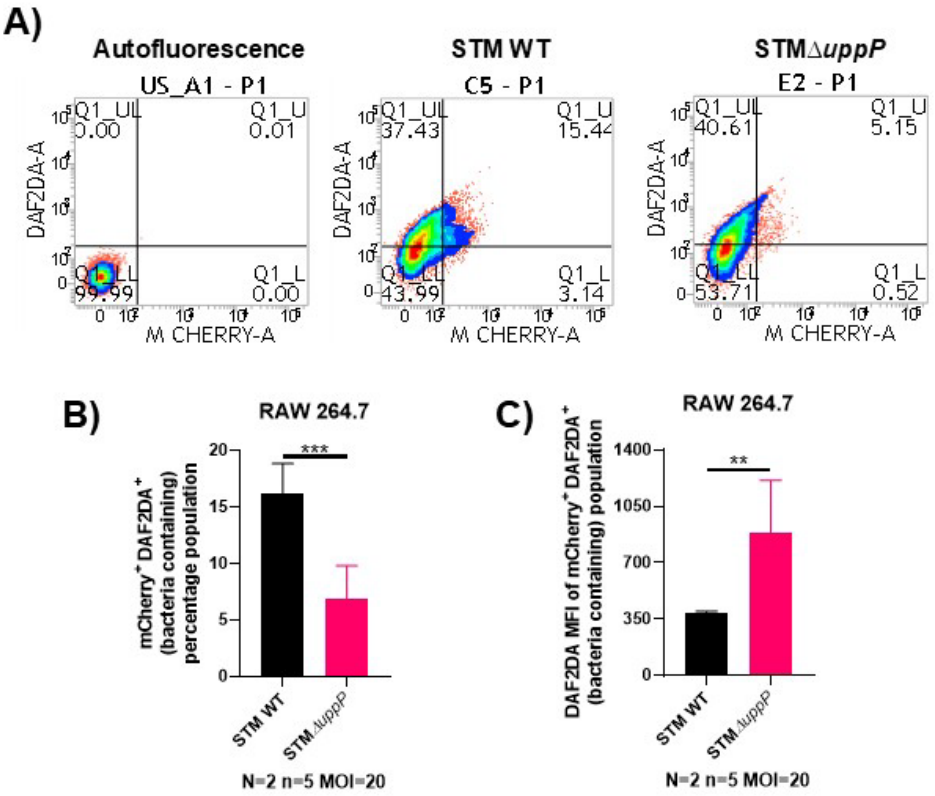

Figure S4. Alternative gating strategy for Fig. 3A-B

A-C) Estimation of nitric oxide in macrophages infected with mCherry-tagged STM WT and STM *ΔuppP* by DAF_2DA staining followed by flow cytometry. Representative DAF_2DA vs mCherry scatter plots of STM WT and STM *ΔuppP* (A). Quantification of mCherry-DAF_2DA double-positive percentage population (B) and DAF_2DA median fluorescence intensity (MFI) (C). Results are representative of N=2, n=4 ± SD. Unpaired two-tailed Student's t-test was performed to obtain the p values. (****P<0.0001, ***P<0.0005, **P<0.001, *P<0.05, ns- non-significant).